Supporting Information
for
“A gate-tunable single-molecule diode”

Mickael L. Perrin,[1] Elena Galán,[2] Rienk Eelkema,[2] Joseph M. Thijssen,[1] Ferdinand Grozema,[2] and Herre S. J. van der Zant[1]

[1]*Kavli Institute of Nanoscience, Delft University of Technology,*
Lorentzweg 1, 2628 CJ Delft, The Netherlands

[2]*Department of Chemical Engineering, Delft University of Technology,*
Julianalaan 136, 2628 BL Delft, The Netherlands

I. TWO-LEVEL MODEL

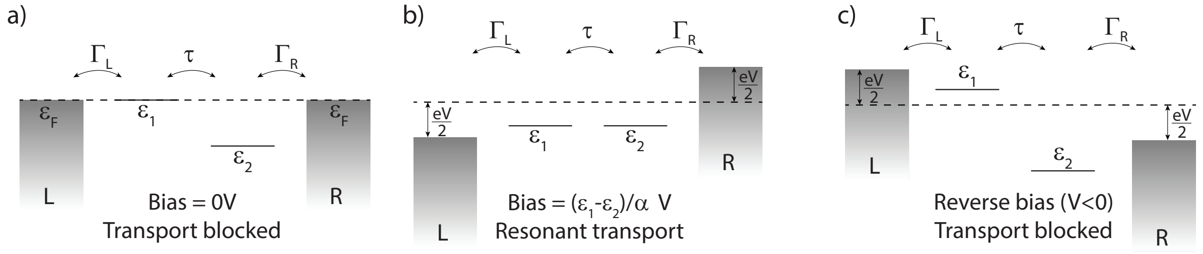

FIG. S.1. **Diode mechanism.** Schematics illustrating charge transport in an asymmetric molecule in the case of (**a**) zero bias, (**b**) forward bias on resonance, (**c**) reverse bias. $\epsilon_{1,2}$ are the on-site energies, τ the inter-site coupling, and α the fraction of the voltage that drops inside the molecule.

The diode mechanism is schematically depicted in Fig. S.1. At zero bias (see Fig. S.1a), the left site is at energy ϵ_1, while the right one is at ϵ_2. As the zero-bias energy splitting (ϵ_1 - ϵ_2) is non-zero, this leads to a low zero-bias conductance. In the model, $\Gamma_{L,R}$ accounts for the electronic coupling of the left (L) and right (R) site to the corresponding electrode. Upon application of a positive bias, the two sites are pulled towards each other as a result of a bias-induced Stark Shift, until they reach a resonant condition at a bias voltage of $V_p = (\epsilon_1 - \epsilon_2)/\alpha$, where α describes the fraction of the voltage that drops inside the molecule. It is important to realize that the voltage drop inside the molecule is essential for the rectification mechanism. Upon approaching the resonance condition, the conductance drastically increases (see Fig. S.1b). For larger bias, the sites are pulled off-resonance again, and the conductance decreases. Therefore, a peak in the current at a bias voltage of V_p is expected. For negative bias, the sites are increasingly pulled away from each other, and the conductance remains low for all voltages (see Fig. S.1c).

The transport properties of such an asymmetric two-site system can be described using the following Hamiltonian

$$= \begin{pmatrix} \epsilon_1 + \frac{1}{2}\alpha eV & -\tau \\ -\tau & \epsilon_2 - \frac{1}{2}\alpha eV \end{pmatrix} . \tag{1}$$

The eigenstates of this Hamiltonian correspond to the bonding (π) and antibonding (π^*) orbitals where their energy splitting Δ in the presence of a bias voltage is given by

$$\Delta = \sqrt{(\alpha eV)^2 + 2\alpha eV(\epsilon_1 - \epsilon_2) + (\epsilon_1 - \epsilon_2)^2 + (2\tau)^2}. \tag{2}$$

We now symmetrically couple the left and right sites to the corresponding leads in the wide-band limit[1,2]:

$$\Gamma_{\mathrm{L}} = \begin{pmatrix} \Gamma & 0 \\ 0 & 0 \end{pmatrix}, \qquad \Gamma_{\mathrm{R}} = \begin{pmatrix} 0 & 0 \\ 0 & \Gamma \end{pmatrix}. \tag{3}$$

The transmission is given by[1–3]

$$\mathcal{T}(\epsilon) = \mathrm{Tr}\left\{\Gamma_{\mathrm{L}} G^r(\epsilon) \Gamma_{\mathrm{R}} G^a(\epsilon)\right\}, \tag{4}$$

where $G^r(\epsilon)$ and $G^a(\epsilon)$ are the retarded and advanced Green's functions, respectively. The former is given by

$$G^r(\epsilon) = \left(\epsilon 1 - H + \frac{\mathrm{i}}{2}\left(\Gamma_{\mathrm{L}} + \Gamma_{\mathrm{R}}\right)\right)^{-1}, \tag{5}$$

while $G^a(\epsilon) = G^r(\epsilon)^\dagger$. The current can be calculated via[1–3]

$$I = \frac{2e}{\hbar} \int \frac{\mathrm{d}\epsilon}{2\pi} \left(f_{\mathrm{L}}(\epsilon) - f_{\mathrm{R}}(\epsilon)\right) \mathcal{T}(\epsilon), \tag{6}$$

where $f_{\mathrm{L}}(\epsilon)$ and $f_{\mathrm{R}}(\epsilon)$ are the Fermi functions of the left and right lead, respectively.

II. DFT + NEGF CALCULATIONS DIODE

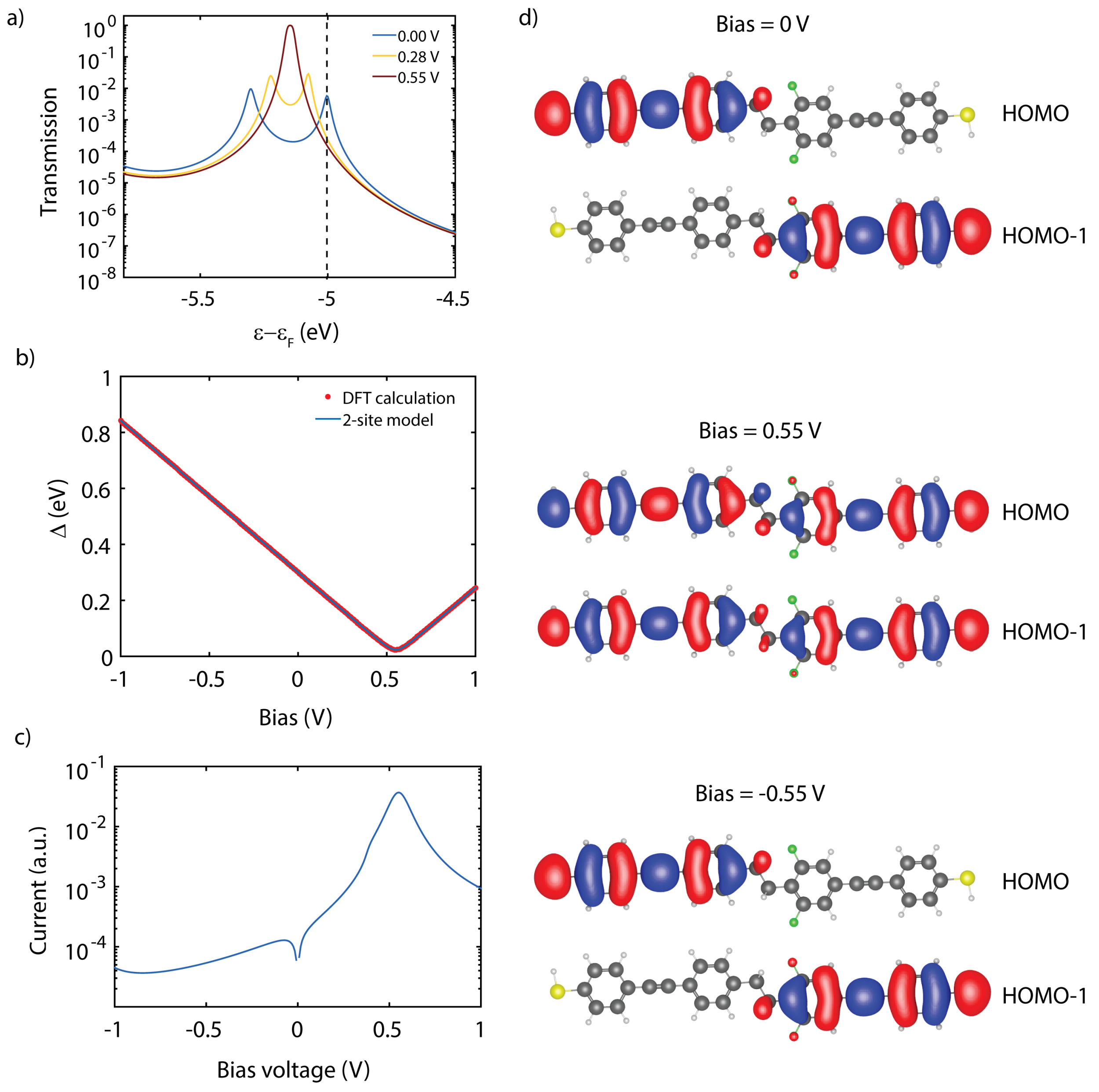

FIG. S.2. **DFT + NEGF calculations on the DPE-2F molecule** (**a**) Transmission for three different bias voltages. (**b**) Energy difference Δ between HOMO and HOMO-1 as calculated from DFT (red). The blue line represents a fit to the two-site model. For more details about the analytical expression, see previous work[4]. (**c**) Current-voltage characteristic calculated using DFT + NEGF plotted on a logarithmic scale. (**d**) Molecular orbitals at zero bias (top), 0.55 V (middle) and -0.55 V (bottom).

Density functional theory (DFT) calculations were performed using the Amsterdam Density Functional (ADF) quantum chemistry package with the GGA PBE exchange-correlation functional and the triple-ζ plus polarization (TZP) basis-set[5,6]. Geometries were converged to energy changes of less than 10^{-3} hartree, energy gradients less than 10^{-3} hartree/Å maximum and $6.7 \cdot 10^{-4}$ hartree/Å RMS. Transmissions were calculated by coupling the p_z-orbitals of the sulphur atoms to wide-band electrodes with a coupling strength of 100 meV. A bias voltage was applied to the molecule by introducing a uniform electric field along the axis connecting the sulphur atoms. The Fermi energy is assumed to be on resonance with the highest occupied molecular orbital (HOMO).

Figure S.2a shows the transmission of DPE-2F for a bias voltages of 0 V, 0.28 V and 0.55 V. At 0 V two peaks in the transmission are visible, corresponding to the HOMO and HOMO-1. They are split by 300 meV, and have a transmission amplitude of $1{\cdot}10^{-2}$. For increasing bias, the peaks increase in amplitude and move towards each other, until at 0.55 V they meet and the transmission reaches unity. The shift in level splitting is made clearer in Fig. S.2b, where the energy splitting between the HOMO and HOMO-1 is plotted. At zero bias, it is 300 meV, and it linearly increases for negative bias. This is the reverse bias as the levels are pulled away from each other. For positive bias, the levels move towards each other and reach a minimum splitting of 23.8 meV at 0.55 V. From this value, the inter-site coupling τ can be calculated to be 16.9 meV. Beyond this voltage, the levels shift away from each other again. The blue line represents a fit of the two-site model[4], from which the model parameters τ, α, ϵ_1 and ϵ_2 can be estimated. The fit reproduces the DFT calculations well. The change in amplitude of the transmission peaks can be understood by considering the orbitals shapes (see Fig. S.2d). For the 0 V and -0.55 V, the HOMO and HOMO-1 are localized on one side of the molecule, leading to poor transport from one sulfur atom to the other. At 0.55 V, on the other hand, the HOMO and HOMO-1 are delocalized, and considering the symmetry of the orbital weight on the sulfur atoms, the transmission goes to unity. The current through the molecule is shown on logarithmic scale in Fig. S.2c. For zero- and negative bias voltages the current is low. It increases for positive bias voltages and reaches a maximum at 0.55 V, after which it decreases again.

As a result of the asymmetry in the current-voltage characteristic, this molecule is expected to behave as a diode, with an operating voltage and peak voltage of 0.55 V, and a rectification ratio of 751. We note that in the calculations the HOMO is assumed to be on resonance with the Fermi energy. In practice, this may not be true, yielding a lower RR.

III. MEASUREMENT ON DPE WITH GATE

In the main text, measurements on the asymmetric DPE-2F molecule are shown. In the case of the DPE, *i.e.*, the molecule with the same backbone but without the electron withdrawing fluorine groups, the molecule is predicted to behave as a resonant tunneling device, with distinct negative differential conductance in the IV characteristics, similar to previous work[7]. For DFT calculations on DPE, we refer to literature[4].

The chemical structure of DPE is shown in Fig. S.3a, with the two conjugated halves marked in green and the broken conjugation in the center marked in red. As discussed in the main text, transport though DPE can be described using a model containing two sites in series, each of them corresponding to a conjugated half. For symmetry reason, the energies of the two sites are equal and correspond to ϵ_0. As for the diode, the sites are weakly coupled to each other by τ and to the left and right lead by Γ_L and Γ_R, respectively.

Figure S.3b presents IVs recorded on a sample with gate exposed to DPE. Four IVs are shown, obtained at different gate voltages. All IVs have a gap at low bias, and an onset in current around ±1 V. Beyond this onset, the current increases and displays a peak around ±1.2 V. This peak is followed by a decrease in current for increasing voltage, *i.e.*, they show negative differential conductance (NDC). The fact that the features in bias occur at opposite polarities is consistent with the symmetric two-site model, having the two sites at a similar energy. From the presence of a gap in the IV, we can deduce that the levels are not on resonance with the Fermi energy at zero bias[7] (ϵ_0 <0). The asymmetry in peak high is most likely due to an asymmetry in Γ.

While sweeping the gate voltage from negative to positive voltages, the gap in the IVs becomes larger. Both the peak current and its position shift towards higher bias voltages. This is more clearly visible in Fig. S.3c, where maps of dI/dV as a function of bias and gate voltage are shown. The top panel zooms in around the peak in the current for positive bias, while the lower panel zooms in at negative bias. In both panels, the black regions at lower bias correspond to the gap, while the bright areas represent the onset of the current. For increasing bias voltage, the differential conductance decreases, until it reaches a black area, corresponding to the peak in the current. Beyond this point, the NDC sets in, visible as a blue area. We note that the shift of the level with gate is consistent with HOMO-mediated charge transport, as expected for this molecule.

Next to the shift of the features (gap, peak, NDC) with gate, the current at the peak is also modulated by the gate. The closer the level is to the Fermi energy, the higher the peak current. Again, this is consistent with calculations performed previously on the same class of molecules[7].

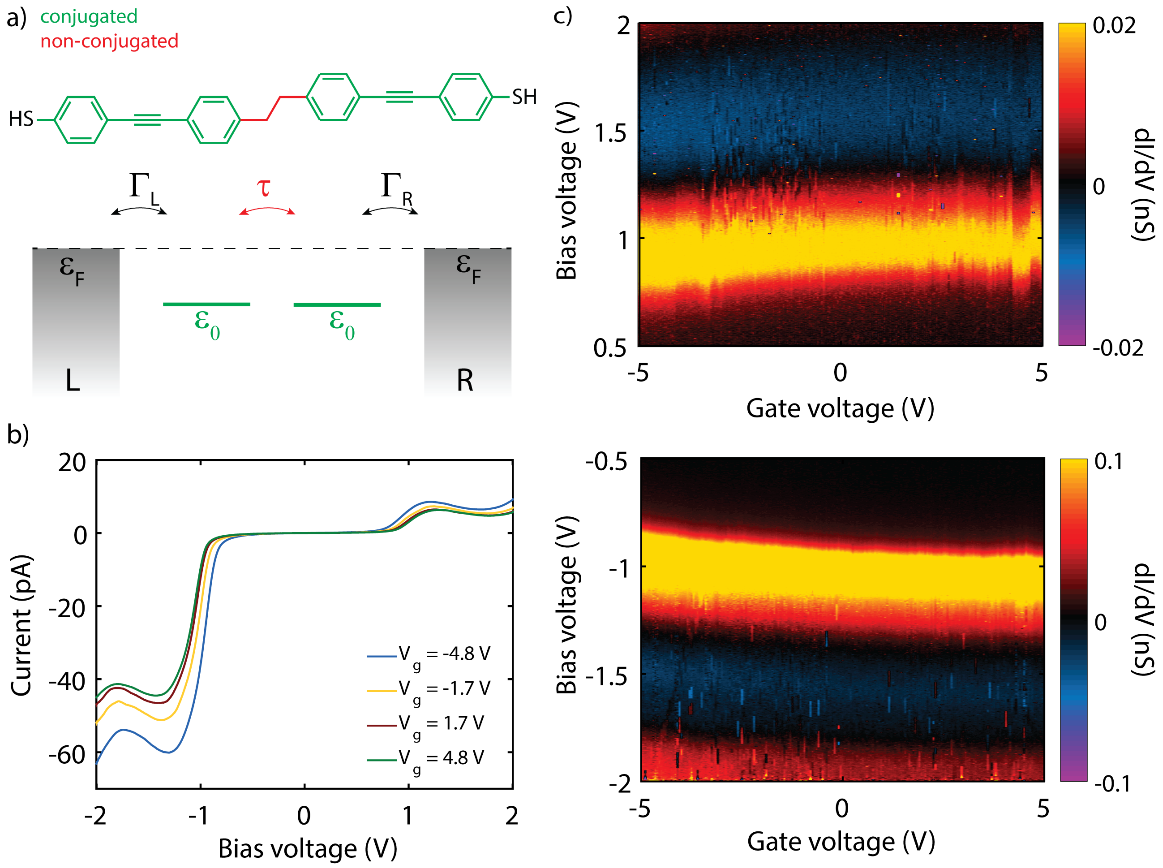

FIG. S.3. **Three-terminal measurements on DPE.** (**a**) Chemical structure of the symmetric DPE molecule, accompanied with a schematic representation of the two-site model. The two halves of the molecule are modelled as two weakly coupled sites in series. For symmetry reasons, the energy of the sites is equal. (**b**) IV charactersitics recorded on DPE for various gate voltages. (**c**) dI/dV map as a function of bias and gate voltage. The plots zoom in around the peak in the current and the NDC at positive (top) and negative (bottom) bias voltage.

IV. SINGLE-LEVEL MODEL

We have also investigated rectification based on an alternative model containing a single-level with asymmetric coupling to the electrodes[8]. In this model, see Fig. S.4a, transport is described using a single level which is positioned at an energy of ϵ_0 below the Fermi energy. This level is then coupled with Γ_L and Γ_R to the left and right electrode, respectively. Transport through such a system can be calculated analytically[9].

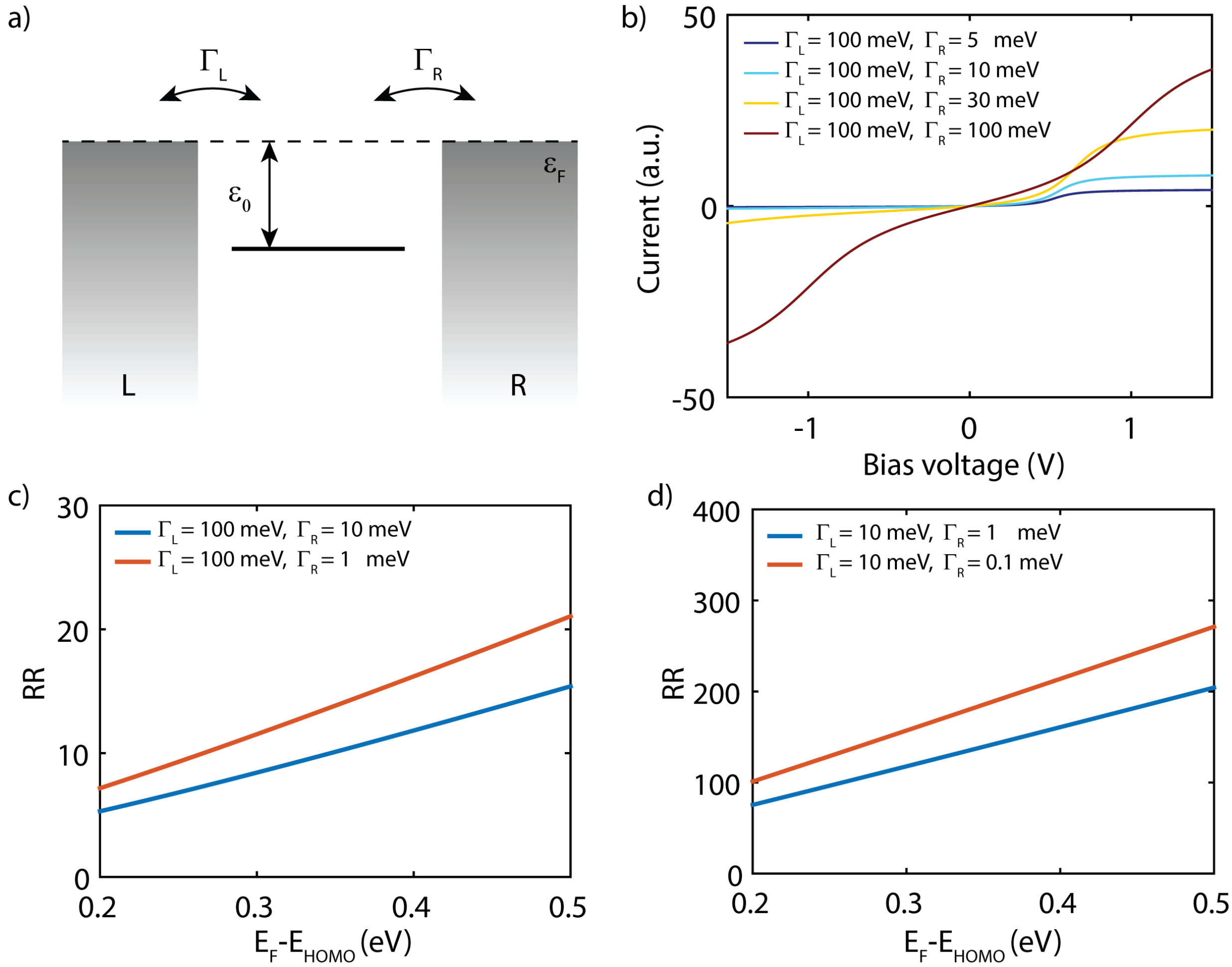

FIG. S.4. **Single-level model calculations.** (**a**) Diagram of a single level located at ϵ_0 away from the Fermi energy, coupled to the two electrodes with $\Gamma_{L,R}$. (**b**) Current-voltage characteristics for four different asymmetries between Γ_L and Γ_R, calculated using the analytical expression[9]. (**c**,**d**) Rectification ratios as a function of level alignment for two asymmetries between Γ_L and Γ_R.

Figure S.4b shows IV characteristics calculated using the single-level model, with Γ_L set to 100 meV, while varying Γ_R between 5 meV and 100 meV. ϵ_0 was set to -0.5 eV, assuming HOMO-mediated transport, as the three-terminal measurements indicate. Figure S.4c presents the extracted RR for an asymmetry of 10 and 100 between Γ_L and Γ_R for level alignments varying between -0.5 eV and -0.2 eV. At -0.5 eV, RR is around 21 for an asymmetry of 100 and around 15 for an asymmetry of 10. For both asymmetries, the RR decreases monotonously when the level is moved towards the Fermi energy, as indicated in Fig. S.4c. Figure S.4d presents the same plot as Fig. S.4c, but with $\Gamma_L = 10$ meV.

Importantly, across a wide range of electronic couplings, the single-level model predicts an increase of RR when shifting the level away from the Fermi energy. This is in contrast with the experiments and the two-level model, in which RR is the highest when on resonance with the Fermi energy[4] and decreases when the level is moved away from it.

V. SINGLE VERSUS TWO-LEVEL MODEL

To emphasize and clarify the opposite trend in rectification as obtained from a single versus two levels, we present Fig. S.5 and Fig. S.6. In the case of the two level model (Fig. S.5), when the HOMO is on resonance with the Fermi energy, $|E_{HOMO}$-$E_F|$=0, the diode performances are optimal with the highest rectification. For $|E_{HOMO}$-$E_F| >0$, the two levels can also align for reverse bias, leading to a non-negligible reverse current and hence a decrease in rectification ratio. Eventually, in the limit of $|E_{HOMO}$-$E_F| >> |\epsilon_1 - \epsilon_2|$, one approaches a symmetric situation with symmetric IVs, in which the rectification ratio will eventually reach unity.

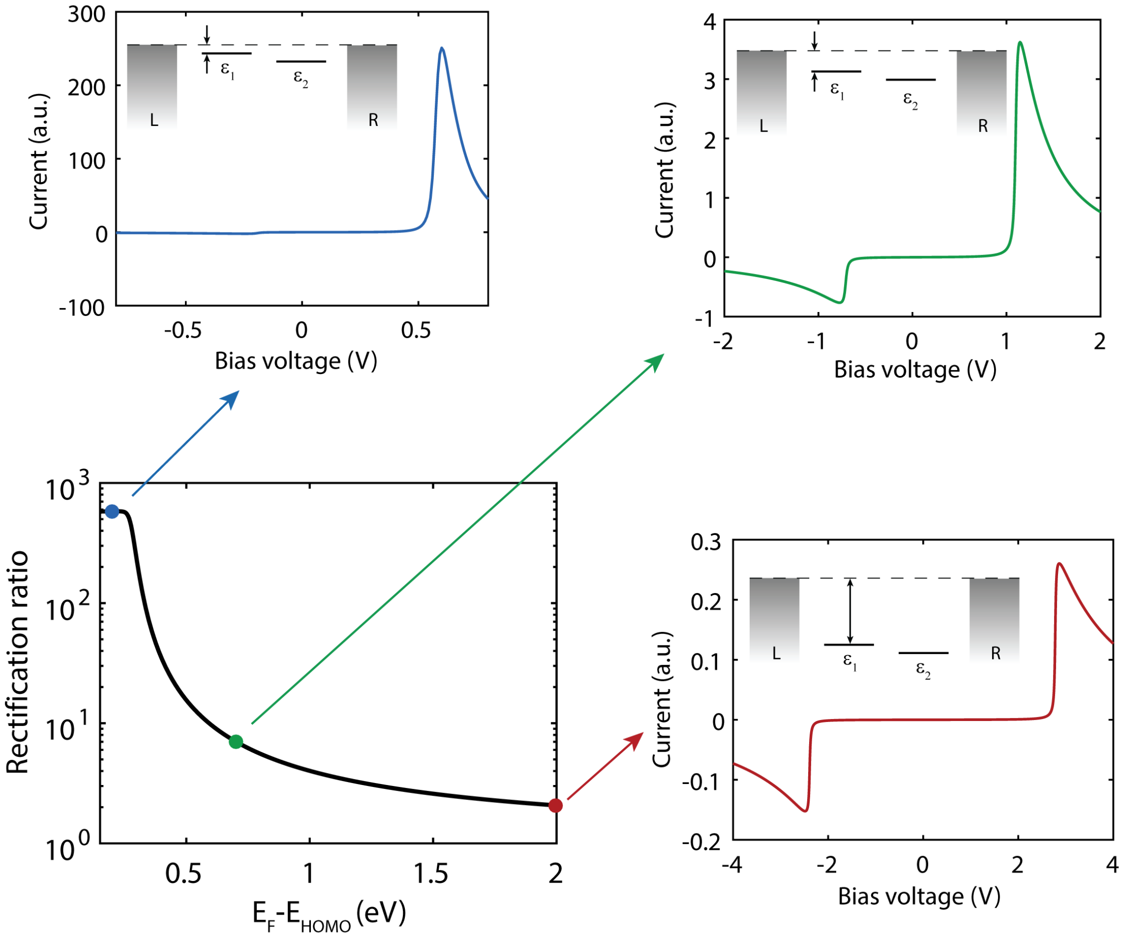

FIG. S.5. **RR and IVs as obtained from the two-level model.** The lower left panel shows the RR for varying level alignment. For this plot the model parameters as shown in Fig. 1 of the main text where used. The remaining three panels show an IV for different level alignments.

In the case of a single level, the situation is opposite, as illustrated in Fig. S.6. At $|E_{HOMO}$-$E_F|$=0, the IV is symmetric, and the rectification is unity. $|E_{HOMO}$-$E_F|$ >0 the asymmetry in the IV starts to develop, increasing thereby the rectification ratio, mainly due to the decrease in reverse bias current. The larger $|E_{HOMO}$-$E_F|$, the larger RR. This trend holds for a large range in asymmetries, even for (unrealistically) high asymmetries in coupling of a factor 100. For the figure below, $\Gamma_L = 1$ meV and $\Gamma_R = 100$ meV. We would like to stress that the trend for a single and two levels are opposite, and the distinction is made by shifting the HOMO with respect to the Fermi energy.

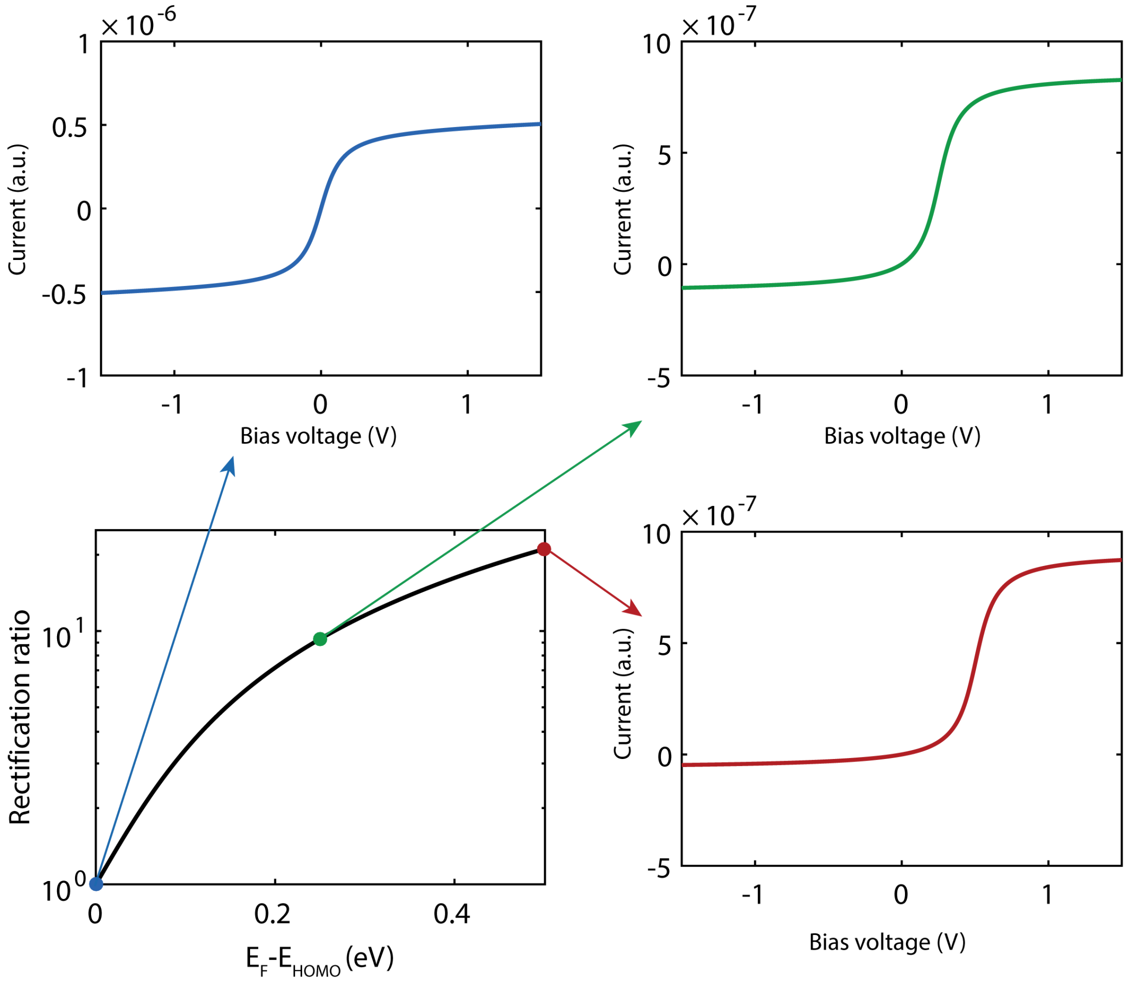

FIG. S.6. **RR and IVs as obtained from the single-level model.** The lower left panel shows the RR for varying level alignment. For this plot we used Γ_L=1 meV and Γ_R=100 meV. The remaining three panels show an IV for different level alignments.

VI. FABRICATION OF THE THREE-TERMINAL SAMPLES

The concept behind three-terminal samples is to fabricate a third electrode that can tune the electrostatic potential of the molecule. The gate electrode is electrically isolated from the source and drain electrodes, and hence couples only electrostatically with the molecule independently from that of the the source/drain electrodes. As a starting point, we have used the recipe published by Martin *et al.*[10]. However, the voltage which can be applied on the gate of those devices is limited to 3 V due to the thickness of the plasma-enhanced native aluminum oxide (Al_2O_3, 2-3 nm). With bias voltages applied between the source/drain up to 2 V, as for instance used in the main text, the gate voltage would be at most 1 V. A way to remedy to this is to increase the breakdown voltage of the gate dielectric, which can be achieved by increasing the oxide thickness. To illustrate this, we assume an increase of the oxide thickness from 3 nm to 8 nm. Assuming a breakdown voltage of 1 V/V, this would result in a breakdown voltage of 8 V. With 2 V applied on the source/drain, the voltage which can be applied on the gate is now 6 V. This is six times higher than in the original design. Even though the gate coupling decreases linearly with oxide thickness, this is outweighted by the much larger gate range.

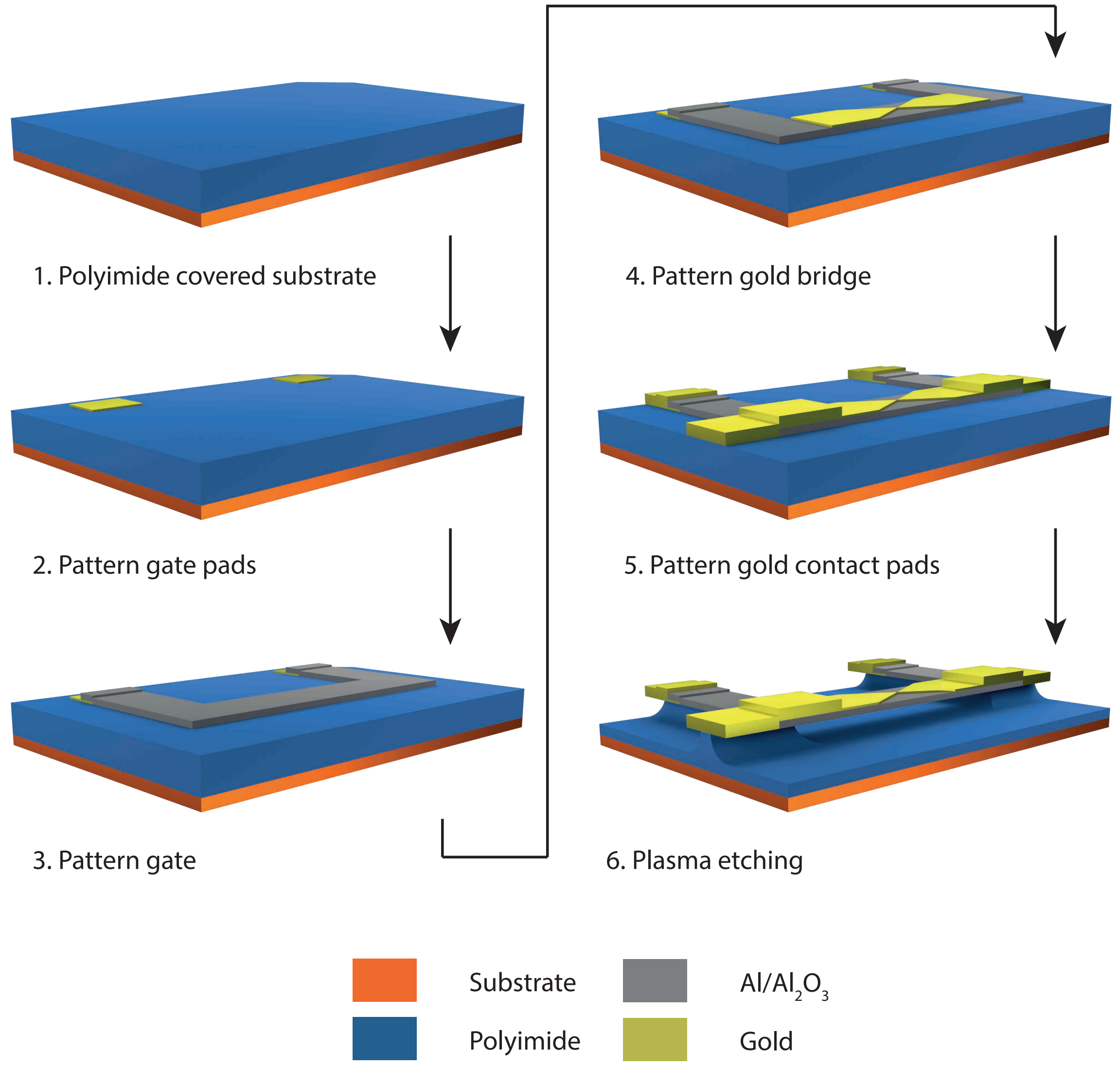

FIG. S.7. **Fabrication steps of gated MCBJ samples.**

What follows below is an improved version of the sandwiched-type three-terminal samples. The higher breakdown voltage has been achieved by increasing the thickness of the gate oxide using atomic layer deposition (ALD). The six fabrication steps are depicted in Fig. S.7 and described in detail below.

Step 1

- As a starting point, polished phosphorous bronze wafers (50x50x0.5 mm) are used. On such a wafer, 10 samples are fabricated.
- Clean the wafers by ultrasonication for 5 min in acetone and isopropanol.
- Apply the adhesion promoter VM651 (HD Microsystems) (soak for 30 s) and spin for 55 s at 3000 rpm.
- Bake for 1 min at 110°C.
- Spin-coat the wafers with polyimide PI2610 (HD Microsystems) for 55 s at 800 rpm.
- Cure the samples for 30 min in a vacuum oven at a temperature of 300°C. The thickness of the resulting polyimide layer is around 6 μm.

Step 2

- Cover the wafer with a methylmethacrylate-methacrylic acid solution (MMA(17.5)MAA 8% in ethyl-L-lactate, Microchem)) and spin-coat for 55 s at 3000 rpm.
- Bake for 7 min at 175 °C. The resulting layer thickness should be around 320 nm.
- Cover the wafer with a PMMA 950k resist solution (4% in anisole, Microchem) and spin-coat for 55 s at 6000 rpm.
- Bake for 7 min at 175 °C. The resulting layer thickness should be around 110 nm.
- Write gate pads and markers with a beam size of 57 nm, a beam step-size of 40 nm and a dose of 750 μC/cm^2.
- Develop the pattern for 90 s in a mixture of methyl-isobutylketone (MIBK) and isopropanol (volume ratio 1:3), followed by 20 s in IPA.

- Electron-beam evaporation of 5 nm of titanium (0.5 Å/s) and 55 nm of gold (1.0 Å/s).

- Lift-off in hot acetone for 1-2 h and rinse with acetone.

Step 3

- Cover the wafer with a methylmethacrylate-methacrylic acid solution (MMA(17.5)MAA 8% in ethyl-L-lactate, Microchem)) and spin-coat for 55 s at 3000 rpm.

- Bake for 7 min at 175 °C.

- Cover the wafer with a PMMA 950k resist solution (4% in anisole, Microchem) and spin-coat for 55 s at 6000 rpm.

- Bake for 7 min at 175 °C.

- Write the gate with a beam size of 3 nm, a beam step-size of 2 nm and a dose of 1100 μC/cm^2.

- Develop pattern for 90 s in a mixture of methyl-isobutylketone (MIBK) and isopropanol (volume ratio 1:3), followed by 20 s in IPA.

- Electron-beam evaporation of 2 nm of titanium (0.5 Å/s) and 80 nm of Al (1.0 Å/s). The chamber pressure should be $<5{\cdot}10^{-7}$mbar to reduce oxidation of aluminum.

- O_2 plasma for 10 s (300 W, 100 mbar, 60 sccm O_2).

- 40 cycles plasma-enhanced atomic layer deposition (Oxford Instruments, 0.12 Å/s) with a stage temperature of 100°C.

- Lift-off in hot acetone for 1-2 h and rinse with acetone.

Step 4

- Cover the wafer with a methylmethacrylate-methacrylic acid solution (MMA(17.5)MAA 8% in ethyl-L-lactate, Microchem)) and spin-coat for 55 s at 3000 rpm.

- Bake for 7 min at 175 °C.

- Cover the wafer with a PMMA 950k resist solution (4% in anisole, Microchem) and spin-coat for 55 s at 6000 rpm.

- Bake for 7 min at 175 °C.
- Write the bridge with a beam size of 3 nm, a beam step-size of 2 nm and a dose of 1100 μC/cm^2.
- Develop the pattern for 90 s in a mixture of methyl-isobutylketone (MIBK) and isopropanol (volume ratio 1:3), followed by 20 s in IPA.
- Electron-beam evaporation of 25 nm of Au (1.0 Å/s). Base pressure $<5\cdot10^{-7}$mbar.
- Lift-off in hot acetone for 1-2 h and rinse with acetone.

Step 5

- Cover the wafer with a methylmethacrylate-methacrylic acid solution (MMA(17.5)MAA 8% in ethyl-L-lactate, Microchem)) and spin-coat for 55 s at 3000 rpm.
- Bake for 7 min at 175 °C.
- Cover the wafer with a PMMA 950k resist solution (4% in anisole, Microchem) and spin-coat for 55 s at 6000 rpm.
- Bake for 7 min at 175 °C.
- The fine leads are written with a beam size of 3 nm, a beam step-size of 2 nm and a dose of 950 μC/cm^2. The coarse leads and the pads are written with a beam size of 82 nm, a beam step-size of 58 nm and a dose of 750 μC/cm^2.
- Develop the pattern for 90 s in a mixture of methyl-isobutylketone (MIBK) and isopropanol (volume ratio 1:3), followed by 20 s in IPA.
- Electron-beam evaporation of 2 nm of titanium (0.5 Å/s) and 120 nm of Al (1.0 Å/s).
- Lift-off in hot acetone for 1-2 h and rinse with acetone.
- Cover the wafer with a PMMA 350k resist solution (3% in anisole, Microchem) and spin-coat for 55 s at 2000 rpm. This layer acts as protection layer during the laser cutting.
- Bake for 2 min at 175 °C.

- The wafers are then cut into individual devices using laser-cutting (ILT Fineworks B.V., Enschede, the Netherlands).

Step 6

- Remove the protection layer by immersion in hot acetone for 10 min.
- Etch the polyimide using a reactive ion etcher with a gas flow of 50 sccm of O_2 gas and 8.5 sccm of CF_4, a pressure of 0.2 mbar and a RF power of 30 W. The resulting oxygen plasma yields a nearly isotropic etch profile with a suspended electrode length of about 2 μm. The etched polyimide is measured *in situ* using an laser interferometer.

VII. CHARACTERISATION OF THE GATE LEAKAGE

To characterize the gate leakage current, an IV was recorded between the gate and the source/drain on a sample fabricated as described above. The measurement was performed on an unbroken bridge; the gate was not broken as well. The resolution in bias voltage was set to 0.3 mV. The scan rate was set to 100 kHz with an averaging of 2000 samples, resulting in an effective sampling rate of 50 Hz. To reduce charging effects due to the very high resistance, a settling time of 80 ms was used for each bias point. Figure S.8 shows the current recorded for voltages between -8 V and 8 V. The leakage current remains below 10 pA, except around -8 V, where it reaches 25 pA. As the onset of the current for negative voltage starts around 7.5 V, the total voltage difference between the source/drain and the gate should not exceed this value.

VIII. DEVICE STATISTICS

In addition to the three-terminal samples, we measured thousands of two-terminal samples, with tens of samples with RRs higher than 100, and up to 500. The spread in RR can be understood from junction-to-junction variations in the level alignment using a simple toy model. Assuming a mean level alignment of 0.5 eV, a standard deviation of 0.1 eV and a junction formation rate of 5-10 percent, out of thousands of junction only tens are expected to yield a RR above 100. This variability may explain the range of RR observed in the experiment. The two-terminal samples, however, are not discussed in more detail. Without

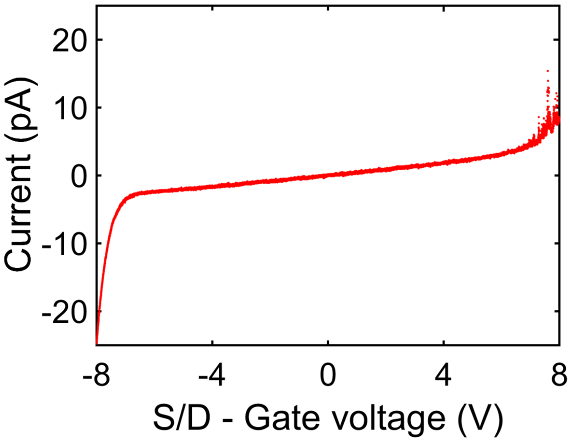

FIG. S.8. **Gate leakage.** IV recorded between the source/drain and the gate.

the presence of the gate electrode, the observed rectification cannot be attributed to the proposed two-site model, the main subject of the paper.

Another proof for the two-level model is the presence of NDC, as this is characteristic of two sites in series, and cannot be reproduced using a single level only. In Fig. S.9 we show IVs recorded on different junction exhibiting a distinct NDC feature.

---

[1] Jauho, A.-P.; Wingreen, N. S.; Meir, Y. *Phys. Rev. B* **1994**, *50*, 5528–5544.

[2] Haug, H.; Jauho, A.-P. *Quantum Kinetics in Transport and Optics of Semiconductors*; Springer, Berlin, Heidelberg, 1997.

[3] Meir, Y.; Wingreen, N. S. *Phys. Rev. Lett.* **1992**, *68*, 2512–2515.

[4] Perrin, M. L.; Galan, E.; Eelkema, R.; Grozema, F. C.; Thijssen, J. M.; van der Zant, H. S. J. *J. Phys. Chem. C* **2015**, *119*, 5697–5702.

[5] te Velde, G.; Bickelhaupt, F. M.; van Gisbergen, S. J. A.; Fonseca Guerra, C.; Baerends, E. J.; Snijders, J. G.; Ziegler, T. *J. Comput. Chem.* **2001**, *22*, 931–967.

[6] Fonseca Guerra, C.; Snijders, J. G.; te Velde, G.; Baerends, E. J. *Theor. Chem. Acc.* **1998**, *99*, 391–403.

[7] Perrin, M. L.; Frisenda, R.; Koole, M.; Seldenthuis, J. S.; Celis Gil, J. A.; Valkenier, H.; Hummelen, J. C.; Renaud, N.; Grozema, F. C.; Thijssen, J. M.; Dulić, D.; van der Zant, H. S. J. *Nat. Nanotechnol.* **2014**, *9*, 830–834.

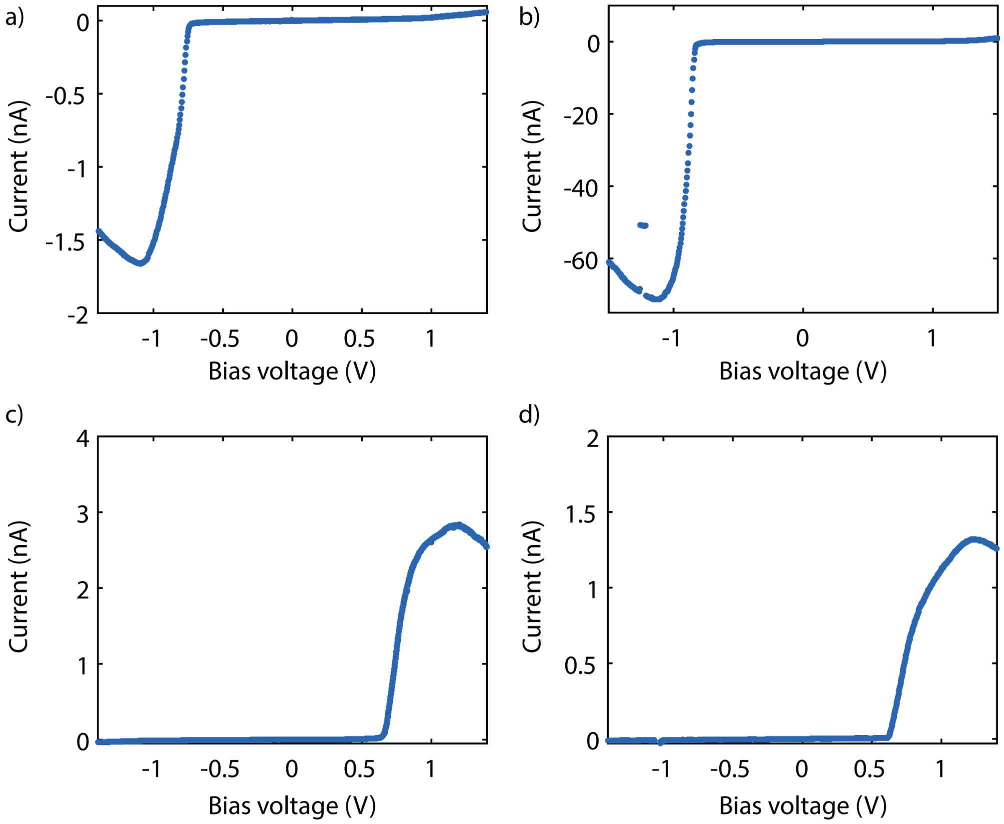

FIG. S.9. **Gate leakage.** IV recorded on different two-terminal junctions, exhibiting NDC.

[8] Kanthasamy, K.; Pfnür, H. *Beilstein J. Nanotechnol.* **2015**,

[9] Frisenda, R.; Perrin, M. L.; Valkenier, H.; Hummelen, J. C.; van der Zant, H. S. J. *Physics Status Solidi B* **2013**, *250*, 2431–2436.

[10] Martin, C. A.; van Ruitenbeek, J. M.; van der Zant, H. S. J. *Nanotechnology* **2010**, *21*, 265201.